

## Subnanosecond Single Electron Source in the Time-Domain

A. Mahé · F.D. Parmentier · G. Fève ·  
J.-M. Berroir · T. Kontos · A. Cavanna ·  
B. Etienne · Y. Jin · D.C. Glattli · B. Plaçais

Received: 23 June 2008 / Accepted: 2 September 2008 / Published online: 21 October 2008  
© Springer Science+Business Media, LLC 2008

**Abstract** We describe here the realization of a single electron source similar to single photon sources in optics. On-demand single electron injection is obtained using a quantum dot connected to the conductor via a tunnel barrier of variable transmission (quantum point contact). Electron emission is triggered by a sudden change of the dot potential which brings a single energy level above the Fermi energy in the conductor. A single charge is emitted on an average time ranging from 100 ps to 10 ns ultimately determined by the barrier transparency and the dot charging energy. The average single electron emission process is recorded with a 0.5 ns time resolution using a real-time fast acquisition card. Single electron signals are compared to simulation based on scattering theory approach adapted for finite excitation energies.

**Keywords** Quantum dot · Single electron source · Subnanosecond quantum dynamics · Two dimensional electron gas · Quantum hall effect

**PACS** 73.21.La · 73.23.-b · 73.43.-f · 85.35.Gv

---

A. Mahé · F.D. Parmentier · G. Fève · J.-M. Berroir · T. Kontos · D.C. Glattli · B. Plaçais (✉)  
Laboratoire Pierre Aigrain, Département de Physique, Ecole Normale Supérieure, 24 rue Lhomond,  
75231 Paris Cedex 05, France  
e-mail: [placais@lpa.ens.fr](mailto:placais@lpa.ens.fr)

D.C. Glattli  
Service de Physique de l'Etat Condensé, CEA Saclay, 91191 Gif-sur-Yvette, France

A. Cavanna · B. Etienne · Y. Jin  
Laboratoire de Photonique et Nanostructures, UPR20 CNRS, Route de Nozay, 91460 Marcoussis  
Cedex, France

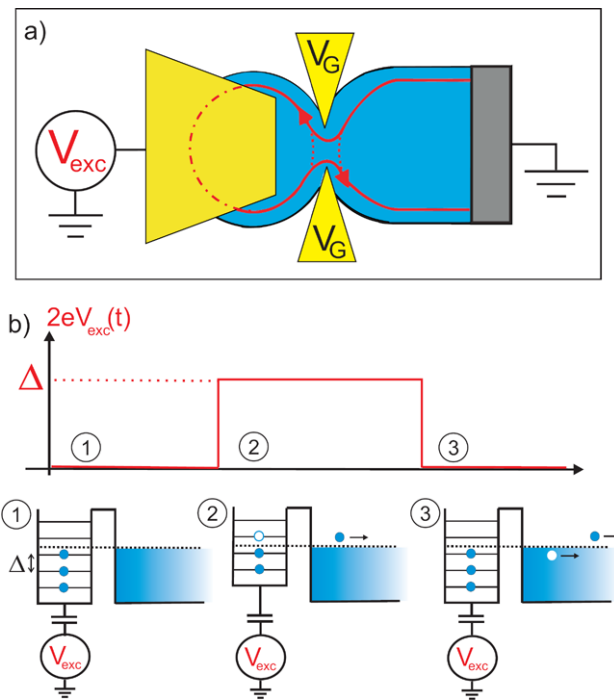


**Fig. 1** (a) Schematic of the circuit. (b) Schematic of single charge injection

## 1 Introduction

The controlled emission of single photons in quantum optics has opened a new route for a quantum information based on entanglement of several photons [1, 2]. Recently, a similar on-demand injection of single electrons in a quantum conductor at a well defined energy, whose uncertainty is ultimately controlled by the tunneling rate has been realized [3, 4]. This experimental realization opens new opportunities for quantum experiments with single electrons [5], including flying qubits in ballistic conductors as envisioned in [6–8]. Of particular relevance is the experiment described in [5] which is an electron collider requiring accurate synchronization of two coherent single electron sources.

We describe here experimental aspects on the realization of such a single electron source [3] and include extended results. Single electron injection is triggered by a sudden variation of the potential of a quantum dot. The electron sitting on the last occupied energy level is then emitted in the lead in a coherent wavepacket, with an energy width limited by the emission time which can be tuned by the QPC transmission  $D$  from 100 picoseconds to 10 nanoseconds.

The circuit, sketched in Fig. 1a, is realized in a 2D electron gas made in a GaAsAl/GaAs heterojunction of nominal density  $n_s = 1.7 \times 10^{15} \text{ m}^{-2}$  and mobility  $\mu = 260 \text{ m}^2 \text{ V}^{-1} \text{ s}^{-1}$ . A quantum dot, of submicron dimensions, is electrostatically coupled to a metallic top gate, located 100 nm above the 2DEG, whose ac voltage amplitude,  $V_{exc}$ , controls the dot potential at the subnanosecond timescale. The dot

is coupled to an electronic reservoir by a quantum point contact (QPC) acting as a tunnel barrier of transmission  $D$  controlled by the gate voltage  $V_g$ . The series addition of both elements constitutes what we call a mesoscopic capacitor or equivalently a quantum RC circuit which is the most basic AC-coupled device exhibiting non-trivial coherent transport properties. For all measurements, the electronic temperature is found about 200 mK for a base fridge temperature in the range 30–70 mK and a magnetic field  $B \approx 1.3$  T is applied to the sample so as to work in the quantum Hall regime (filling factor  $\nu = 4$ ) with no spin degeneracy. We think that the difference between electronic and fridge temperatures mainly comes from unperfect gate voltage filtering.  $V_g$  is tuned to control the transmission  $D$  of a single edge state from the reservoir to the dot. It also controls by capacitive coupling the mean potential of the dot.

In the linear response regime to a high frequency potential excitation applied to the top gate, the mesoscopic circuit forms a quantum RC circuit. The study of the charge relaxation is described in [9, 10] where it was demonstrated the quantization of the charge relaxation resistance  $R_q = h/2e^2$  for a single mode conductor with no spin degeneracy predicted ten years before [11–13]. The total capacitance of the dot is the series addition of the geometrical capacitance  $C$  and the quantum capacitance  $C_q = e^2 N(\epsilon_f)$  where  $N(\epsilon_f)$  is the density of states of the dot at the Fermi energy. As in our experiment we have  $C \gg C_q$ , the charge relaxation time  $\tau_q \simeq R_q C_q = h N(\epsilon_f)/2$  is a new indirect measurement of the density of states. Importantly for the present work, the linear response allows for a precise extraction of the parameters of the dot: level spacing  $\Delta \approx 2$  K, geometrical capacitance  $C \approx 3$  fF, and the total addition energy  $E_c = \Delta + e^2/C = 2.5$  K. As capacitance effects are dominated by the quantum capacitance  $C_q$ , we shall neglect the geometrical capacitance in the rest of the paper and take  $E_c \equiv \Delta$ . Kinetic inductance effects in the leads give rise to additional time delays [14, 15] which can be neglected in our small structures. We also disregard here possible decoherence effects beside thermal smearing due to finite reservoir temperature. For a theoretical discussion on interactions and finite coherence time effects on the charge relaxation process the reader is referred to [16, 17].

This paper deals with the regime of high excitation amplitudes comparable with the level spacing  $\Delta \approx 200$  μeV. By applying a sudden step voltage on the top gate, the first occupied energy level of the dot is brought above the Fermi energy of the reservoir and a single electron is emitted (see Fig. 1b) on a characteristic time  $\tau$  which is expected to be related to the width of this single energy level,  $\tau = h/D\Delta$ . In this experiment the emission time,  $\tau = h/D\Delta$ , was larger than the pulse rise time ( $\sim 50$  ps) so that the lifting of the energy level can be regarded as instantaneous. This emission time  $\tau$  differs in general from the above charge relaxation time  $\tau_q$  of the coherent regime. However, it coincides with the charge relaxation time in the incoherent regime as observed at high temperatures and/or low transmissions ( $k_B T \gg D\Delta$ ) [9]. Multiple charge emission is prevented by both Coulomb interactions and Pauli exclusion principle. In this work single charge detection is achieved by statistical averaging of a large number of events. To repeat the experiment, the dot needs to be reloaded by putting the potential back to its initial value. One electron is then absorbed by the dot, or equivalently a hole is emitted in the Fermi sea. Periodic repetition of square voltage excitations then generates periodic emission of single electron-hole pairs which

leads to a quantized ac-current in units of  $2ef$  [3, 4]. This is a marked difference with pumps which show quantization of the dc current in units of  $ef$  [18].

This periodic current can be measured either by phase resolved harmonic measurements [3] or directly in the time domain with a fast acquisition and averaging card (Acqiris AP240 2GSa/s). In this paper, we will focus on this second measurement scheme.

## 2 Current Pulses in the Time Domain

The average current generated by single charge transfer is detected in time domain by the voltage drop on a  $50\ \Omega$  resistor located at the input of a broadband low noise cryogenic amplifier. Given an escape time  $\tau \approx 500\ \text{ps}$ , the input voltage amplitude is  $V \approx (50\ \Omega) \times e/\tau \approx 16\ \text{nV}$ . For a  $15\ \text{K}$  noise temperature amplifier in a  $1\ \text{GHz}$  bandwidth, the input noise amplitude is a few  $\mu\text{V}$ . Single shot measurement of single charges is thus out of reach. Only statistical measurements of the average current can be achieved. The experiment needs to be repeated about  $10^5$  times to restore a signal to noise ratio close to unity with our current setup.

Although each electron is detected at a well defined time, single electron emission is a quantum probabilistic process. We thus expect that the average current resulting from the accumulation of a large set of single electron events will reconstruct the probability density of electronic emission. As in a usual decay process, it should follow an exponential relaxation on a characteristic time given by the escape time  $\tau$ . This exponential relaxation can be viewed in the lumped elements language as the mere relaxation time of a RC circuit. A current pulse with opposite sign is expected for the single hole emission.

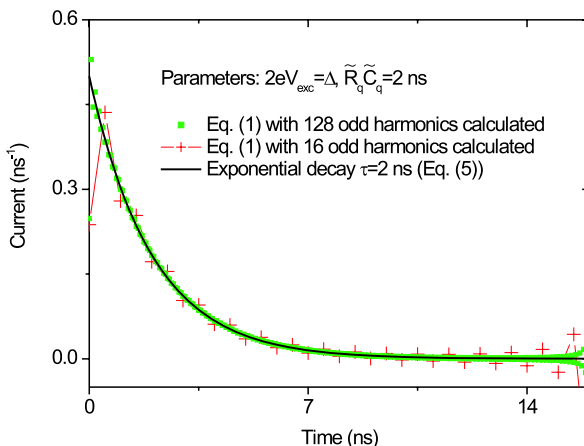
The expected current can be theoretically calculated by a scattering theory approach similar to that of [13] extended to high excitations amplitudes, while neglecting interactions as discussed above [3]. Further developments include estimation of source quantization accuracy and noise [19] and the emission of secondary electron-hole pairs [20, 21]. As a single edge state is transmitted to the dot, we will consider below a single mode conductor with no spin degeneracy. Odd harmonics of the current  $I_{(2k+1)\omega}$  can be written as [22]

$$\begin{aligned} I_{(2k+1)\omega} = & \frac{e}{2\pi i\hbar} \frac{1}{2k+1} \int d\epsilon [1 - s^+(\epsilon)s(\epsilon + (2k+1)\hbar\omega)] \\ & \times [f(\epsilon + (2k+1)\hbar\omega) + f(\epsilon) - f(\epsilon - 2eV_{exc} + (2k+1)\hbar\omega) \\ & - f(\epsilon - 2eV_{exc})], \end{aligned} \quad (1)$$

where  $2V_{exc}$  is the peak to peak amplitude of the excitation voltage and  $s(\epsilon)$  is the energy-dependent scattering parameter. At low frequency  $(2k+1)\omega \ll 1/\tau$ , the current can be expanded up to the second order in  $(2k+1)\omega$ :

$$\begin{aligned} I_{(2k+1)\omega} = & \frac{i2V_{exc}}{\pi(2k+1)} \int d\epsilon \left[ -i(2k+1)\omega e^2 N(\epsilon) + \frac{\hbar}{2e^2} [e^2 N(\epsilon)(2k+1)\omega]^2 \right] \\ & \times \frac{f(\epsilon - 2eV_{exc}) - f(\epsilon)}{2eV_{exc}} \end{aligned} \quad (2)$$

**Fig. 2** Comparison between (1) and (5) for the calculation of the current. Both expressions coincide when a large number of harmonics are calculated. Deviations at short times are observed when only 16 harmonics are taken into account



where the prefactor is the  $(2k + 1)$ th harmonic of the excitation voltage, and the density of states  $N(\epsilon)$  is related to the scattering matrix through  $N(\epsilon) = 1/(2i\pi) \times s(\epsilon)ds^+(\epsilon)/d\epsilon$ . The above equation thus establishes that the circuit is equivalent to an RC circuit with a  $V_{exc}$ -dependent capacitance and resistance given by:

$$\tilde{C}_q = e^2 \int d\epsilon N(\epsilon) \frac{f(\epsilon - 2eV_{exc}) - f(\epsilon)}{2eV_{exc}} \quad (3)$$

$$\tilde{R}_q = \frac{h}{2e^2} \frac{\int d\epsilon N(\epsilon)^2 \frac{f(\epsilon - 2eV_{exc}) - f(\epsilon)}{2eV_{exc}}}{[\int d\epsilon N(\epsilon) \frac{f(\epsilon - 2eV_{exc}) - f(\epsilon)}{2eV_{exc}}]^2}. \quad (4)$$

In the time domain, this corresponds to an exponentially decaying current:

$$I(t) = \frac{q}{\tau} e^{-t/\tau}, \quad \text{with } q = \tilde{C}_q \times 2V_{exc}, \quad \text{and} \quad \tau = \tilde{R}_q \tilde{C}_q \quad (5)$$

Equation (3) shows that the charge  $q$  is given by the density of states integrated between the extremum values of the square excitation. If one energy level initially located below the Fermi energy is brought above the Fermi sea, then a single charge is transferred as naively predicted. In the limit of low transmissions  $D \ll 1$ , (3) and (4) give a relaxation time  $\tau \approx h/D\Delta$  as anticipated.

Comparison in Fig. 2 between the exact expression of the current (1) and its low frequency limit, (2) and (5) (escape time  $\tau = 2$  ns), validates the low-frequency approximation. Therefore, we shall only consider this simpler form from now on.

Even harmonics can also be calculated although their expressions are more involved. They reveal the possible differences between the electron and hole emission processes which are disregarded in our measurement procedure as discussed below.

Experimentally one can only access to a finite number of current harmonics. In our case, the current is recorded using a 1 GHz fast averaging card. With a drive frequency of 31.25 MHz, 32 harmonics can be measured (16 odd harmonics). One can see in Fig. 2 that this bandwidth limitation hardly affects the relaxation process for  $\tau \geq 1$  ns.

The measurement setup will now be detailed in the next section.

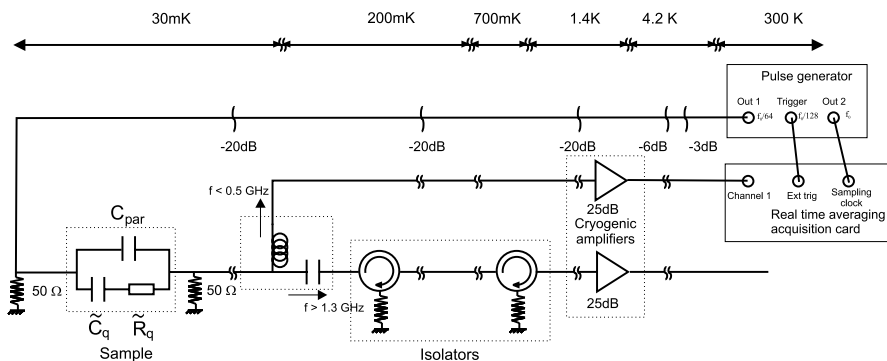


**Fig. 3** Schematic of the experimental setup

### 3 Experimental Setup

An input square excitation of approximately 1 V amplitude and 50 ps risetime is provided by a pulse generator at frequency 31.25 MHz and fed at the input of a 40 GHz rf-transmission line. After an attenuation of  $\approx 70$  dB, it reduces to a square signal of a few hundreds of microvolts applied to a  $50\ \Omega$  resistor at the gate of the sample, see Fig. 3. Two ultra low noise cryogenic amplifiers record the voltage drop on another  $50\ \Omega$  resistor located at the output of the sample. A bias tee separates the low frequency ( $< 500$  MHz) part of the current signal from the high frequency ( $> 1.3$  GHz) part. The high frequency line is used to measure the harmonic response of the sample for a high frequency drive (typically 1.5 GHz) as described in [3]. We will focus here on the low frequency part from which we extract the time domain dependence of the current for a 31.25 MHz drive. The first measurement scheme gives access to ultra short times ( $\approx 10$  ps resolution) whereas the second method gives the complete time dependence of the current but on longer times ( $> 500$  ps). Note that all the spectrum cannot be measured by a single amplifier as the sample is protected from the high frequency part of the amplifiers current noise by the use of rf-isolators with limited bandwidth 1.2–1.8 GHz.

A fast averaging card (Acqiris AP240) of 1 GHz bandwidth (sampling time 500 ps) records the output current. Averaging over long times (a few seconds) requires a perfect synchronisation of the sampling clock with the drive frequency. Therefore, the sampling clock is generated by the generator and the drive is an integer fraction of the clock:  $f_{drive} = 2\text{ GHz}/64 = 31.25\text{ MHz}$  (see Fig. 3). One run of measurements is triggered every 4096 periods of the drive (so that one run lasts 100  $\mu\text{s}$ ). Typically 65000 runs are then averaged by the card in real time for a total measurement time of  $\approx 10$  s. The overall procedure gives a signal to noise ratio  $\sim 10$  in a 1 GHz bandwidth.

As mentioned before, the effective bandwidth of the detection line is limited to 500 MHz by the first bias tee. The cryogenic amplifiers also suffer from a low frequency cutoff of a few tens of MHz. Moreover, impedance mismatch of the amplifiers leads to multiple reflections (echoes) which also affect the measured time dependence

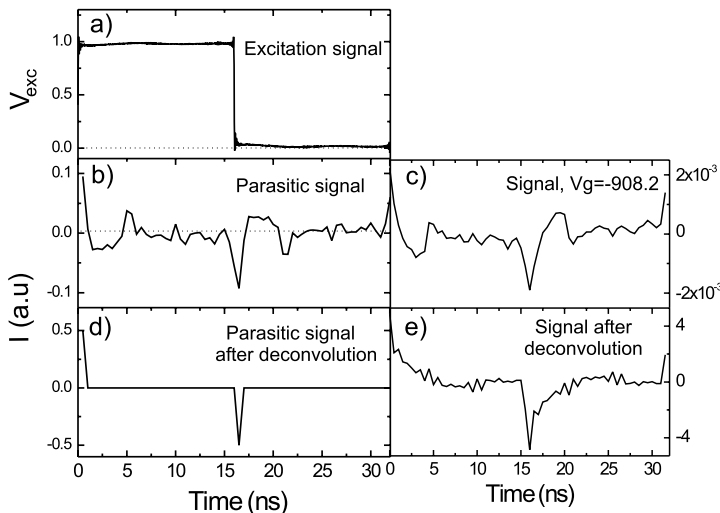


**Fig. 4** Excitation, parasitic and sample contribution signals (a), (b) and (c). Panels (d) and (e) show the parasitic and sample signals after deconvolution of the amplification line response

of the signal. Finally the current signal is affected by bandwidth limitations and distortion. However, these spurious effects can be corrected by proper calibration.

As seen previously, the sample can be represented by the series addition of a resistance and capacitance given by (3) and (4). However, it is always bypassed by a parasitic capacitive coupling  $C_{par}$ , see Fig. 3. In our setup it corresponds to the largest part of the transmitted current ( $C_{par} \approx 50 \text{ fF}$  compared to  $\tilde{C}_q \approx 0.7 \text{ fF}$ ). By varying the gate voltage  $V_g$ , the quantum dot can be decoupled from the electronic reservoir (at transmission  $D = 0$ ,  $R_q = \infty$ ), allowing for an accurate measurement of the parasitic contribution which is then subtracted to only keep the sample contribution. This parasitic signal can be used as a reference signal for the detection line. Indeed for a capacitive coupling, the voltage drop on the output  $50 \Omega$  resistor is given by an exponential relaxation on time  $RC \ll 500 \text{ ps}$ . It can thus be approximated by a Dirac delta function compared to the  $500 \text{ ps}$  sampling time of the card. Therefore, the Fourier transform of the parasitic contribution gives an accurate measurement of the odd Fourier components of the detection line bandwidth. The pristine signal can be reconstructed by dividing its odd measured Fourier components by those of the detection line. As even components cannot be calibrated, they are disregarded in this experiment. This amounts to disregard differences in the electron and hole emission processes. A typical measured parasitic signal is given on Fig. 4b where one can see the previously mentioned distortions (widening caused by the  $500 \text{ MHz}$  bandwidth, drop to negative values of current after a positive peak caused by the low frequency cutoff and echoes). The effect of the deconvolution process on a typical trace can then be seen on Fig. 4e; most of the distortions have been erased and one recovers an exponential decrease of the current.

The next section will now describe the main results obtained with this measurement setup.

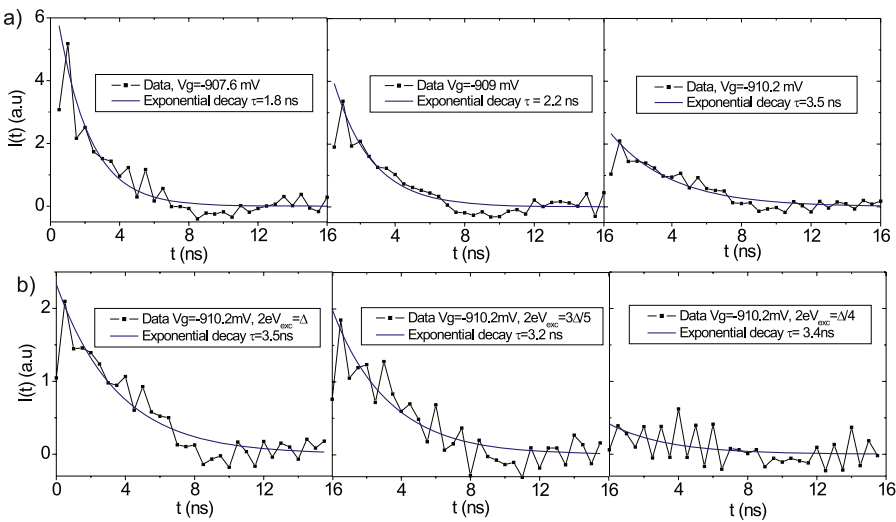


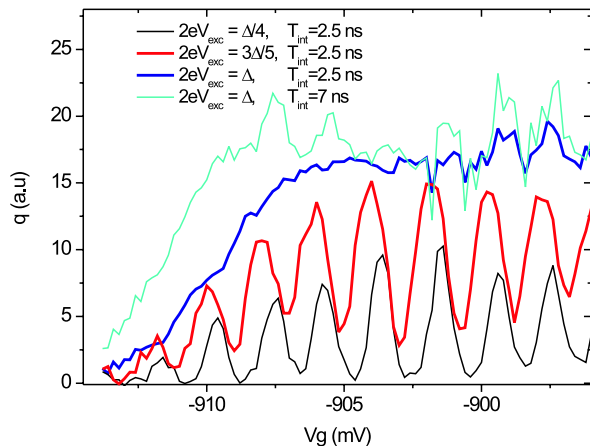
**Fig. 5** (a) Data and exponential fits for  $V_g = -907.6$ ,  $-909$  and  $-910.2$  mV, and an excitation amplitude of  $2eV_{exc} = \Delta$ . (b) Data and exponential fits at  $V_g = -910.2$  mV for  $2eV_{exc} = \Delta$ ,  $3\Delta/5$  and  $\Delta/4$

## 4 Results

Figure 5a presents a few typical current pulses obtained for  $2eV_{exc} \approx \Delta$  for different values of the gate voltage corresponding to different transmissions. For lower values of the gate voltage, the transmission decreases and the escape time increases as predicted by (5). Moreover, all these curves are well fitted by an exponential relaxation from which the escape time  $\tau$  can be extracted.  $\tau$  can be continuously varied within two orders of magnitude, from a hundred of picoseconds to ten nanoseconds by a simple shift in the gate voltage  $V_g$ . By contrast, in this regime of low transmissions, the escape time does not depend much on the excitation amplitude as can be seen on Fig. 5b. Again this behavior is expected as for  $h/\tau \ll k_B T$ , the linear regime relaxation time  $\tau_q$  averaged on the energy window  $k_B T$  coincides with the high excitation value  $h/D\Delta$ .

The averaged transmitted charge in a given time can be obtained by integrating the current pulse over a given time window. Figure 6 represents the average transmitted charge in a window of 2.5 ns for three excitation amplitudes  $2eV_{exc} = \Delta/4$ ,  $3\Delta/5$ ,  $\Delta$ . For  $2eV_{exc} = \Delta/4$ , the transmitted charge exhibits strong oscillations with gate voltage. In some cases, the excitation amplitude is not high enough to promote an energy level above the Fermi energy and the transferred charge is zero. On the opposite, when a level is close to resonance the transmitted charge shows a peak. When the excitation amplitude is increased these structures tend to disappear up to the level  $2eV_{exc} = \Delta$  for which the transmitted charge does not depend on gate voltage anymore (except for low values of gate voltage as the escape time becomes longer than the integration time). In this case one electron is transferred independently of the initial value of the dot potential. It is the time-domain counterpart of the quantized ac current  $I_\omega = 2ef$  in the harmonic measurement reported in [3].

**Fig. 6** Average charge transferred in the first 2.5 ns for  $2eV_{exc} = \Delta/4$ ,  $3\Delta/5$  and  $\Delta$  and after  $T_{int} = 7$  ns for  $2eV_{exc} = \Delta$



One can also see that the peaks observed for  $2eV_{exc} = 3\Delta/5$  are very close to the curve obtained for  $2eV_{exc} = \Delta$ . In this case, the transmitted charge has a very small dependence on the excitation amplitude. It exhibits a quantized plateau as only a single charge can be emitted at each period of the drive. One can also see that for a longer integration window of 7 ns, the curve obtained for  $2eV_{exc} = \Delta$  is shifted to lower transmissions as expected. At the same time, high transmission part of the curve becomes more noisy as the integration window incorporates more noise.

Finally all the results obtained for different values of the gate voltage and excitation amplitude can be represented on a two-dimensional colorplot, Fig. 7, where the current is represented in colorscale. We observe again at low amplitudes the periodic oscillations reflecting the periodicity of the dot density of states (horizontal axis). Broadening of the current peaks occurs at low transmission as the escape time becomes longer (vertical axis). For  $2eV_{exc} = \Delta$ , the oscillations vanish as one electron is emitted at each period and one can only observe the variation of escape time with gate voltage. The right part of Fig. 7 represents numerical simulations using (1) with no adjustable parameters (level spacing and transmission are extracted from the linear measurements at low amplitudes). The experimental behavior is very well reproduced in the numerical simulations in the nanosecond scale of the time resolved experiment.

## 5 Conclusion

We have reported here on the measurement in the time domain of time controlled single electron emission using fast acquisition and averaging techniques. Such a single electron source together with single electron detection [23] would open the way to quantum electron optics experiments probing electron antibunching or electron entanglement [5, 24].

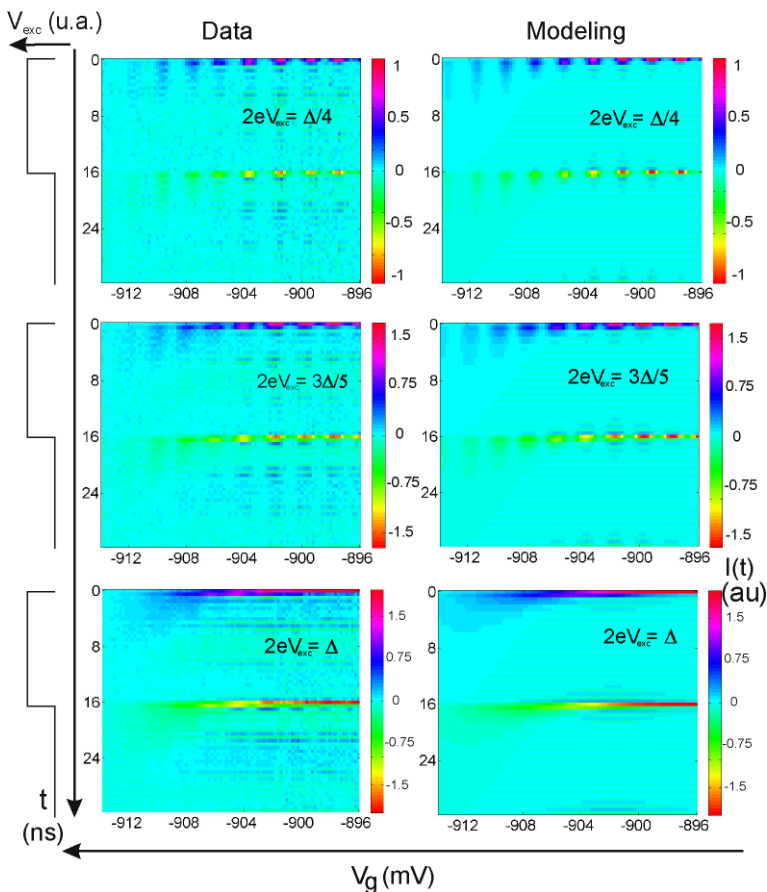


**Fig. 7** Two-dimensional plot of the current represented in colorscale as a function of time (*vertical axis*) and gate voltage (*horizontal axis*). The current is plotted for  $2eV_{exc} = \Delta/4$ ,  $3\Delta/5$  and  $\Delta$  experimental data are plotted and the *left side*, numerical simulations on the *right*. Excitation pulses are displayed on the *left* so as to emphasize synchronization of electron/hole emission with the rising/falling edge of the pulses. Difference between experiment and model lies mainly in the presence of ripples at finite time delays which we attribute to imperfections in the deconvolution process

**Acknowledgement** The Laboratoire Pierre Aigrain is the CNRS-ENS mixed research unit (UMR8551) associated with universities Paris 6 and Paris 7. The research has been supported by the ANR-05-NANO-028 contract.

## References

1. N. Gisin, G. Ribordy, W. Tittel, H. Zbinden, Rev. Mod. Phys. **74**, 145–195 (2002)
2. P. Kok et al., Rev. Mod. Phys. **79**, 135–174 (2007)
3. G. Fève, A. Mahé, J.-M. Berroir, T. Kontos, B. Plaçais, A. Cavanna, B. Etienne, Y. Jin, D.C. Glattli, Science **316**, 1169 (2007)
4. G. Fève, A. Mahé, J.-M. Berroir, T. Kontos, B. Plaçais, D.C. Glattli, A. Cavanna, B. Etienne, Y. Jin, Physica E **40**, 954 (2008)

5. S. Ol'khovskaya, J. Splettstoesser, M. Moskalets, M. Büttiker, Shot noise of a mesoscopic two-particle collider. *Phys. Rev. Lett.* **101**, 166802 (2008)
6. A. Bertoni, P. Bordone, R. Brunetti, C. Jacoboni, S. Reggiani, *Phys. Rev. Lett.* **84**, 5912–5915 (2000)
7. R. Ionicioiu, G. Amaralunga, F. Udrea, *Int. J. Mod. Phys.* **15**, 125–133 (2001)
8. T.M. Stace, C.H.W. Barnes, G.J. Milburn, *Phys. Rev. Lett.* **93**, 126804–126807 (2004)
9. J. Gabelli, G. Fèvre, J.-M. Berroir, B. Plaçais, A. Cavanna, B. Etienne, Y. Jin, D.C. Glattli, *Science* **313**, 499–502 (2006)
10. J. Gabelli, G. Fèvre, J.-M. Berroir, B. Plaçais, Y. Jin, B. Etienne, D.C. Glattli, *Physica E* **34**(1–2), 576 (2006). (Proceedings of EP2DS-16)
11. M. Büttiker, H. Thomas, A. Prêtre, *Phys. Lett. A* **180**, 364–369 (1993)
12. M. Büttiker, A. Prêtre, H. Thomas, *Phys. Rev. Lett.* **70**, 4114–4117 (1993)
13. A. Prêtre, H. Thomas, M. Büttiker, *Phys. Rev. B* **54**, 8130 (1996)
14. J. Gabelli, G. Fèvre, T. Kontos, J.-M. Berroir, B. Plaçais, D.C. Glattli, B. Etienne, Y. Jin, M. Büttiker, *Phys. Rev. Lett.* **98**, 166806 (2007)
15. J. Wang, B.G. Wang, H. Guo, *Phys. Rev. B* **75**, 155336 (2007)
16. S.E. Nigg, R. Lopez, M. Büttiker, *Phys. Rev. Lett.* **97**, 206804 (2006)
17. S.E. Nigg, M. Büttiker, *Phys. Rev. B* **77**, 085312 (2008)
18. M.D. Blumenthal, B. Kaestner, L. Li, T.J.B.M. Janssen, M. Pepper, D. Anderson, G. Jones, D.A. Ritchie, *Nat. Phys.* **3**, 343–347 (2007)
19. M. Moskalets, P. Samuelsson, M. Büttiker, *Phys. Rev. Lett.* **100**, 086601 (2008)
20. J. Keeling, A.V. Shytov, L.S. Levitov, [arXiv:0804.4281](https://arxiv.org/abs/0804.4281) (2008)
21. J. Keeling, I. Klich, L.S. Levitov, *Phys. Rev. Lett.* **97**, 116403 (2006)
22. G. Fèvre, Thesis, Université Pierre et Marie Curie, Paris (2006). Available at <http://tel.archives-ouvertes.fr/tel-00119589>
23. G. Fèvre, P. Degiovanni, T. Jolicoeur, *Phys. Rev. B* **77**, 035308 (2008)
24. F. Hassler, G.B. Lesovik, G. Blatter, *Phys. Rev. Lett.* **99**, 076804 (2007)